Acta Crystallographica Section F
**Structural Biology Communications**
ISSN 2053-230X

# Structure of *Mycobacterium tuberculosis* nucleoside diphosphate kinase R80N mutant in complex with citrate

**Florian Georgescauld,[a,b]* Lucile Moynié,[a,b] Johann Habersetzer[a,b] and Alain Dautant[a,b]***

[a]Institut de Biochimie et de Génétique Cellulaires, UMR 5095, CNRS, 1 Rue Camille Saint-Saëns, 33077 Bordeaux, France, and [b]Institut de Biochimie et de Génétique Cellulaires, UMR 5095, Bordeaux University, 1 Rue Camille Saint-Saëns, Bordeaux, France

Correspondence e-mail: fgeorges@biochem.mpg.de, a.dautant@ibgc.cnrs.fr

Received 5 December 2013
Accepted 18 December 2013

**PDB reference:** nucleoside diphosphate kinase, R80N mutant, 4ane

The crystal structure of the wild-type nucleoside diphosphate kinase from *Mycobacterium tuberculosis* at 2.6 Å resolution revealed that the intersubunit salt bridge Arg80–Asp93 contributes to the thermal stability of the hexamer ($T_m$ = 76°C). On mutating Asp93 to Asn to break the salt bridge, the thermal stability dramatically decreased by 27.6°C. Here, on mutating Arg80 to Asn, the thermal stability also significantly decreased by 8.0°C. In the X-ray structure of the R80N mutant solved at 1.9 Å resolution the salt bridge was replaced by intersubunit hydrogen bonds that contribute to the thermal stability of the hexamer. A citrate anion from the crystallization buffer was bound at the bottom of the nucleotide-binding site *via* electrostatic and hydrogen-bonding interactions with six conserved residues involved in nucleotide binding. Structural analysis shows that the citrate is present at the location of the nucleotide phosphate groups.

## 1. Introduction

Nucleoside diphosphate kinase (NDPK) is an essential enzyme for the synthesis of non-adenine nucleoside (and deoxynucleoside) 5′-triphosphates. NDPK catalyzes the reversible transfer of the γ-phosphate of nucleoside triphosphates to nucleoside diphosphates (Janin & Deville-Bonne, 2002). NDPKs form hexamers or tetramers (Moynié *et al.*, 2007). 3′-Phosphorylated nucleotides (Schneider *et al.*, 1998) and cAMP analogues (Strelkov *et al.*, 1995; Anciaux *et al.*, 1997) are known inhibitors of NPDK activity. Although NDPK can function as a protein kinase (Wagner & Vu, 1995), it has been convincingly demonstrated in *Escherichia coli* that phosphotransferase activity is mediated by ADP (Levit *et al.*, 2002).

The crystal structure of the wild-type *Mycobacterium tuberculosis* NDPK (*Mt*-NDPK; PDB entry 1k44) revealed the presence of an intersubunit salt bridge, Arg80–Asp93, which was missing in NDPKs from other organisms (Chen *et al.*, 2002). To check the significance of this salt bridge in the high thermal stability of the hexamer, Arg80 or Asp93 was mutated to a neutral asparagine. Previously, denaturation studies using temperature and chaotropic reagents showed that the D93N mutation dramatically decreases the stability of the hexamer. In the crystal structures of the D93N mutant (PDB entries 4anc and 4and), Arg80 and Asn93 were not involved in any intersubunit interactions (Georgescauld *et al.*, 2013).

Here, the R80N mutation was introduced. Unexpectedly, the hexamer stability was very different on mutating one or the other of the amino acids forming the bridge. In the crystal structure of the R80N mutant refined at 1.9 Å resolution (PDB entry 4ane), the side chain of Asn80 forms two strong intersubunit hydrogen bonds. This new crystal structure explains why the wild-type (WT) and R80N *Mt*-NDPK hexamers display higher stability compared with the D93N hexamer. A citrate anion was bound in the active site, making ten interactions with protein ligands, including six direct interactions. Although inhibition of NDPK by citrate has never been reported *in vivo*, such a possibility cannot be excluded.

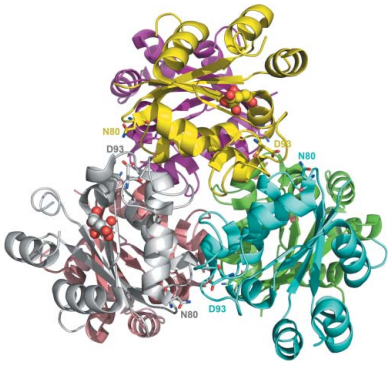

## 2. Materials and methods

### 2.1. Macromolecule production

The experimental procedures have been described elsewhere (Georgescauld *et al.*, 2013).

### 2.2. Crystallization

The protein solution was dialysed against 20 m*M* Tris–HCl pH 7.5 buffer containing 20 m*M* $MgCl_2$ and concentrated to 11 mg ml$^{-1}$. The drops were prepared by mixing equal amounts (200 + 200 nl) of the protein and reservoir solutions using a Honeybee 961 robot (Cartesian Technology). Crystals of the R80N mutant grew at 20°C in a few hours using condition No. 86 of The Classics Suite (Qiagen) consisting of 30%(*w*/*v*) PEG 4000, 0.2 *M* ammonium acetate, 0.1 *M* trisodium citrate pH 5.6. The crystals were cryoprotected in mother liquor supplemented with 20%(*v*/*v*) glycerol and flash-cooled in liquid nitrogen.

**Table 1**
Summary of data collection and processing.

| | |
|---|---|
| Diffraction source | Beamline ID23-1, ESRF |
| Wavelength (Å) | 0.97625 |
| Temperature (K) | 107 |
| Detector | ADSC CCD |
| Space group | *I*2 |
| Unit-cell parameters (Å, °) | *a* = 68.82, *b* = 113.34, *c* = 107.56, $\alpha$ = 90, $\beta$ = 106.40, $\gamma$ = 90 |
| Resolution range (Å) | 32.90–1.90 (1.93–1.90) |
| No. of unique reflections | 57601 (2141) |
| Completeness (%) | 92.9 (83.7) |
| Multiplicity | 1.9 (1.8) |
| $\langle I/\sigma(I)\rangle$ | 7.80 (3.6) |
| $R_{\rm r.i.m.}$† | 0.087 (0.210) |
| Overall *B* factor from Wilson plot (Å$^2$) | 21.02 |

† Estimated $R_{\rm r.i.m.} = R_{\rm merge} \times [N/(N-1)]^{1/2}$, where $N$ is the data multiplicity.

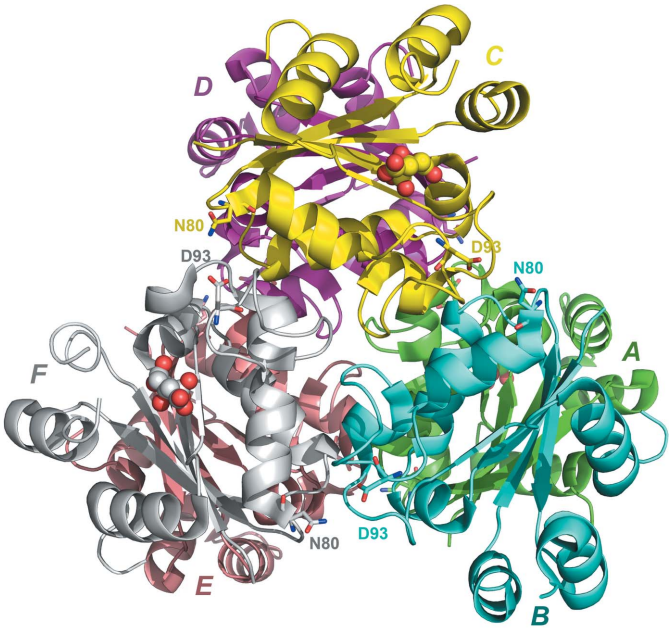


**Figure 1**
Cartoon representation of the biologically relevant hexameric structure of R80N mutant *Mt*-NDPK coloured by chain and viewed along the threefold symmetry axis. The Asn80 (the mutation site) and Asp93 residues are drawn as sticks, while citrate molecules bound in the active site are drawn as spheres. The chains are labelled *A*–*F*.

### 2.3. Data collection and processing

Diffraction data were collected at 107 K on beamline ID23-1 at ESRF, Grenoble. The data were processed with *MOSFLM* (Leslie, 2006) and scaled with *SCALA* (Winn *et al.*, 2011). The data-collection statistics are summarized in Table 1.

### 2.4. Structure solution and refinement

The crystal belonged to space group *I*2 and contained six molecules in the asymmetric unit. The structure was determined by the molecular-replacement method with *MOLREP* (Vagin & Teplyakov, 2010) using the coordinates of the WT *Mt*-NDPK structure as the search model (PDB entry 1k44; Chen *et al.*, 2002). Refinement was performed using *phenix.refine* in *PHENIX* (Adams *et al.*, 2010) alternated with manual model building in *Coot* (Emsley & Cowtan, 2004). Noncrystallographic symmetry (NCS) restraints were implemented during refinement, excluding residues 44–64, with positional

**Table 2**
Structure-refinement statistics.

| | |
|---|---|
| Resolution range (Å) | 29.651–1.900 (1.9328–1.9000) |
| Completeness (%) | 92.6 |
| $\sigma$ Cutoff | $F > 0.00\sigma(F)$ |
| No. of reflections, working set | 57601 (2141) |
| No. of reflections, test set | 2927 (102) |
| Final $R_{\rm cryst}$ | 0.184 (0.2395) |
| Final $R_{\rm free}$ | 0.235 (0.3295) |
| No. of non-H atoms | |
| Protein | 5933 |
| Ligand | 39 |
| Water | 448 |
| Total | 6420 |
| R.m.s. deviations | |
| Bonds (Å) | 0.009 |
| Angles (°) | 1.078 |
| Average *B* factors (Å$^2$) | |
| Protein | 32.6 |
| Ligand | 52.5 |
| Water | 34.5 |
| Ramachandran plot (%) | |
| Favoured regions | 97.8 |
| Additionally allowed regions | 1.9 |
| Outliers | 0.1 |

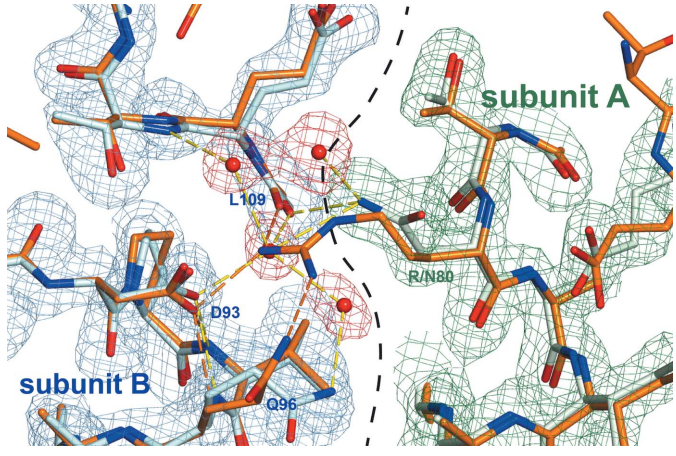


**Figure 2**
Superimposition of the WT and R80N mutant *Mt*-NDPK structures at the subunit interface. The intersubunit salt bridge Arg80–Asp93 found in WT *Mt*-NDPK (PDB entry 1k44) was replaced by intersubunit hydrogen bonds in the R80N mutant involving the side-chain atoms of residues 93 and 96 and the main-chain carbonyl of Leu109 (PDB entry 4ane). The C atoms of WT and R80N mutant *Mt*-NDPK are coloured orange and white, respectively. The $2F_{\rm o} - F_{\rm c}$ electron densities contoured at $2\sigma$ for chains *A* and *C* and water molecules of the R80N structure are coloured dark green, blue and red, respectively. The interface is marked with a broken line.

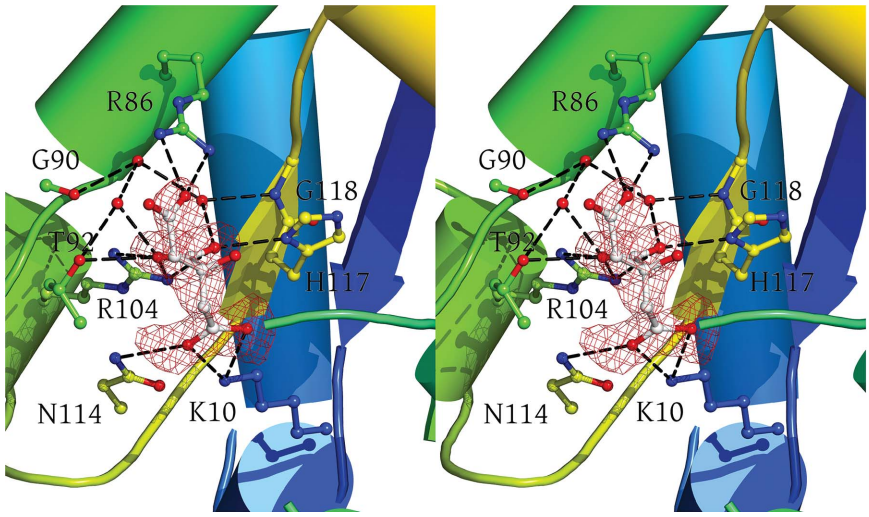


**Figure 3**
Stereoview of the difference electron-density/OMIT ($F_o - F_c$) map at a 2.0$\sigma$ contour level showing the fit of the citrate in the active site of the R80N mutant *Mt*-NDPK structure. The protein ligands of the citrate are drawn as sticks (see also Supporting Fig. S3). The cartoon representation of the protein is coloured in a rainbow ramp from blue at the N-terminus to red at the C-terminus.

weights of 0.1 and thermal weights of 10.0. TLS groups were designated using the *TLSMD* server (Painter & Merritt, 2006). In the final model, a few residues belonging to the short loop connecting helices $\alpha_A$ and $\alpha_2$ (residues 56–58, 55–58 and 54–61 in chains *B*, *D* and *F*, respectively) were absent owing to poor electron density in these regions. The $F_o - F_c$ maps revealed electron density for citrate in the active site. The occupancy factor of citrate was fixed at 1. Atomic coordinates and experimental structure factors for R80N mutant *Mt*-NDPK at 1.9 Å resolution have been deposited in the PDB as entry 4ane. The figures were produced using *PyMOL* (DeLano, 2002). The stereochemistry of the R80N mutant *Mt*-NDPK structure was good as assessed by *MolProbity* (Chen *et al.*, 2010). The refinement statistics are summarized in Table 2.

## 3. Results and discussion

The thermal denaturation of WT *Mt*-NDPK and its R80N and D93N mutants was followed by differential scanning calorimetry. The $T_m$ was 76.0°C and 68°C for *Mt*-NDPK and the R80N mutant, respectively, while it drastically decreased to 48.4°C for the D93N mutant (Supporting Fig. S1[1]). Similar $T_m$ values were obtained on measuring the enzyme inactivation for each protein, suggesting simultaneous dissociation/unfolding (data not shown). Since Arg80 and Asp93 interact *via* an intersubunit salt bridge, a neutral molecule (urea) or a salt (guanidinium hydrochloride) was used as a chemical denaturant. For the WT protein and the R80N mutant, the unfolding and the loss of quaternary structure occurred simultaneously (Supporting Fig. S2), while the D93N mutation lowered the stability of the hexamer to urea denaturation since the hexamer first dissociates into monomers before unfolding (Georgescauld *et al.*, 2013). The salt bridge is clearly involved in the stability of the hexamer. However, such large differences in melting temperature and in behaviour towards chemical denaturation for the R80N and D93N mutants constituted a puzzling result. To gain insights into the structural basis of these differences, crystal structure determinations were carried out.

The *Mt*-NDPK R80N mutant crystallized in a monoclinic space group with 47% solvent content, while the WT and the D93N mutant crystallized in orthorhombic space groups with 56–68% solvent content. Thus, the R80N mutant crystals diffracted to significantly higher resolution (1.8 Å) than the WT crystals (2.6 Å). The overall structures of the monomer (r.m.s.d. of 0.6 Å for $C^\alpha$ atoms) and the hexamer (r.m.s.d. of 0.9 Å for $C^\alpha$ atoms) are essentially unaltered by the R80N mutation (Fig. 1). Compared with the WT structure, the $\alpha_A$–$\alpha_2$ helical loop of every chain is 10° more tilted towards the central $\beta$-sheet, closing the catalytic pocket, independent of the presence of citrate and of crystal-packing interactions. At the trimeric interface, relative to the WT, the inter-subunit salt bridge Arg80–Asp93 was obviously lost. However, similarly to Arg80, Asn80 is hydrogen-bonded to the main-chain carbonyl of Leu109 of the neighbouring subunit and moreover to the Asp93 carboxyl group *via* a water molecule (Fig. 2). The other intersubunit hydrogen bonds present in the WT (Lys29 to the carbonyl of Pro94, Gly105 and Gly108; Arg16 to the carbonyl of Arg28) are conserved in the R80N mutant. This explains why the stability of the R80N hexamer is less disturbed compared with that of the D93N hexamer.

Among the six subunits in the asymmetric unit, three subunits (*A*, *D* and *F*) have a bound citrate in the active site. The citrate anion is docked *via* electrostatic and hydrogen-bonding interactions with six conserved residues: a lysine (Lys10), two arginines (Arg86 and Arg104), a threonine (Thr92), an asparagine (Asn114) and the catalytic histidine (His117) (Fig. 3). It is also hydrogen-bonded to the main-chain N atom of Gly118 and to the His49, His50, Tyr50 and Thr92 side chains through a water molecule. All of the O atoms of the three carboxyl groups and the hydroxyl group are involved in binding. The citrate binding does not appears to be linked to the R80N mutation. Although citrate fits well in the active site and occupies the same location as the nucleotide phosphate groups, a crystal structure of WT or mutant NDPK in complex with citrate has never been reported.

Pr Ioan Lascu and Pr Anna Giartosio are acknowledged for their support and helpful discussions. The authors wish to thank the beamline staff at the ESRF, Grenoble, France for their help in performing X-ray diffraction. This project was supported by the ESRF.

[1] Supporting information has been deposited in the IUCr electronic archive (Reference: HV5248).

## References


Adams, P. D. *et al.* (2010). *Acta Cryst.* D**66**, 213–221.
Anciaux, K., Van Dommelen, K., Willems, R., Roymans, D. & Slegers, H. (1997). *FEBS Lett.* **400**, 75–79.
Chen, V. B., Arendall, W. B., Headd, J. J., Keedy, D. A., Immormino, R. M., Kapral, G. J., Murray, L. W., Richardson, J. S. & Richardson, D. C. (2010). *Acta Cryst.* D**66**, 12–21.
Chen, Y., Morera, S., Mocan, J., Lascu, I. & Janin, J. (2002). *Proteins*, **47**, 556–557.
DeLano, W. L. (2002). *PyMOL.* http://www.pymol.org.
Emsley, P. & Cowtan, K. (2004). *Acta Cryst.* D**60**, 2126–2132.
Georgescauld, F., Moynié, L., Habersetzer, J., Cervoni, L., Mocan, I., Borza, T., Harris, P., Dautant, A. & Lascu, I. (2013). *PLoS One*, **8**, e57867.
Janin, J. & Deville-Bonne, D. (2002). *Methods Enzymol.* **354**, 118–134.
Laskowski, R. A. & Swindells, M. B. (2011). *J. Chem. Inf. Model.* **51**, 2778–2786.
Leslie, A. G. W. (2006). *Acta Cryst.* D**62**, 48–57.
Levit, M. N., Abramczyk, B. M., Stock, J. B. & Postel, E. H. (2002). *J. Biol. Chem.* **277**, 5163–5167.
Moynié, L., Giraud, M.-F., Georgescauld, F., Lascu, I. & Dautant, A. (2007). *Proteins*, **67**, 755–765.
Painter, J. & Merritt, E. A. (2006). *J. Appl. Cryst.* **39**, 109–111.
Schneider, B., Xu, Y. W., Janin, J., Véron, M. & Deville-Bonne, D. (1998). *J. Biol. Chem.* **273**, 28773–28778.
Strelkov, S. V., Perisic, O., Webb, P. A. & Williams, R. L. (1995). *J. Mol. Biol.* **249**, 665–674.
Vagin, A. & Teplyakov, A. (2010). *Acta Cryst.* D**66**, 22–25.
Wagner, P. D. & Vu, N. D. (1995). *J. Biol. Chem.* **270**, 21758–21764.
Winn, M. D. *et al.* (2011). *Acta Cryst.* D**67**, 235–242.